INTERNATIONAL JOURNAL OF MARITIME TECHNOLOGY
IJMT Vol.3/ Winter 2015 (49-60)
Available online at: http://ijmt.ir/browse.php?a_code=A-10-66-2&sid=1&slc_lang=en

Field Measurements and 3D Numerical Modeling of Hydrodynamics in Chabahar Bay, Iran

Mohsen Soltanpour[1*], Mohammad Dibajnia[2]

[1*]*Civil Eng. Department, K. N. Toosi University of Technology, Tehran, Iran; soltanpour@kntu.ac.ir*
[2]*Baird & Associates, Canada; mdibajnia@baird.com*

ARTICLE INFO

Article History:
Received: 21 Oct. 2014
Accepted: 14 Apr. 2015
Available online: 20 Jun. 2015

Keywords:
Field Measurements
Hydrodynamics
MISED 3D model
Particle tracking
Chabahar Bay

ABSTRACT

As the first phase of a series of monitoring and modeling studies of Iranian coastal areas, Chabahar Bay, located on the north coast of the Gulf of Oman, was under a comprehensive monitoring and modeling study in 2006-2007. The study included an extensive one-year field measurements program to help understanding the ongoing processes in the bay and provide inputs or boundary conditions and validation data for numerical models. An analysis of the collected data and the results of three-dimensional (3D) hydrodynamic numerical modeling are described in this paper. 3D numerical model of MISED was employed to provide a full spatial picture of bay-wide circulations and its sensitivity to environmental factors such as tides and winds. MISED simulations were completed for the months of February and March 2007 and the results were compared with the measurements. It was observed that the simulated tidal currents favorably agree with the measured data at the selected stations. Particle tracking simulations using a Lagrangian Particle Tracking Model showed that the combination of wind-driven and tidal currents generates a self-flushing function that tends to carry suspended material to outside of the bay. The combination of winds and tides has thus a very important assimilative function for water quality of Chabahar Bay.

1. Introduction

Gulf of Oman is the water body that connects the Arabian Sea to the Strait of Hormuz, which then runs to the Persian Gulf. Similar to the currents in the North Indian Ocean, the currents in the Gulf of Oman are also affected by monsoon winds (Shankar et al., 2002). Although Indian Ocean circulation and the currents of Arabian Sea have been partially studied during past decades (e.g., Duing 1970; Flagg and Kim 1998; Swapna 2005), there is no published attempts to present current patterns in the Gulf of Oman.

Chabahar Bay is a large Omega-shaped (Ω) bay with two headlands located on the north coast of the Gulf of Oman in south-eastern Iran. As this part of the Iranian coastline faces the open sea, most of the coasts receive persistent swell waves arriving from the south. The coastline also comes under the influence of the south-western monsoon. The bay is one of several crenulated-shape (Ω) bays along this coastline where a number of semi-natural ports have been constructed (Figure 1). These bays are formed when transgressive seas, during phases of rapid sea level rise, breach ranges of barrier mountains or highland outcrops protecting low-lying inland areas floored by easily-erodible sediments. They have a smooth curve shape that has two distinct sections, i.e. the curve section in the lee of upcoast headland and a tangent section joining curve section to the downcoast headland. Different phrases have been used to name these bays such as headland-bay beaches (Le Blond, 1979), hooked beaches (Rea and Komar, 1975) and crenulate-shaped bays (Silvester and Ho, 1972), etc.

Chabahar Bay is part of Makran area which is considered to be tectonically active. Some previous works suggest that the Chabahar region has been tectonically uplifted throughout the Quaternary, at the rate of approximately 0.2 mm/year (e.g., Falcon 1947; Reyess et al. 1998; Vita-Finzi 2002). Pozm Headland on the west side of the bay with an elevation of 104 m is the most significant result of this uplift in the region. Figure 2 shows the bathymetry of the bay. The highland outcrops are shown on both sides of Chabahar Bay entrance in this figure. These are Pozm Headland on the west side and Chabahar Headland on the east side. Water depth along the entrance of the bay is about 14 m relative to Chart Datum (CD). The east half and particularly the southeast corner of the bay are rather deep and suitable for navigation.

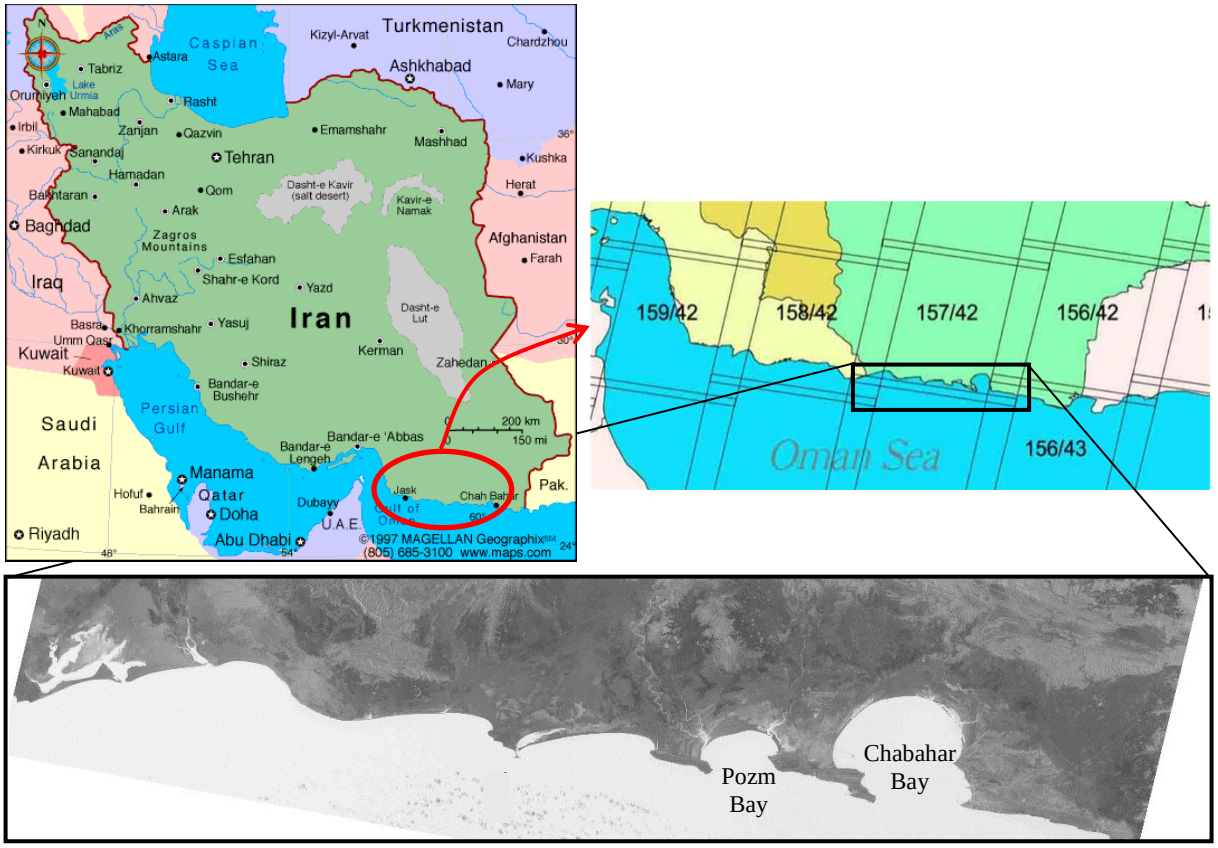

Figure 1. A chain of crenulate-shaped bays at southeast of Iran

Chabahar Bay has an important role in the region and many marine projects have been constructed in the bay. The most recent and important development on the southeast corner of the bay involves construction of the 2.5 km long Shaheed Beheshti Port breakwater which extends from the tip of Chabahar Headland out to about 12 m depth. A number of commercial, military and fishery ports are also located in the southeast part of the bay. The west half of the bay, on the contrary, features shallow areas and very mild slopes. Konarak Fishery Port jetty on this side of the bay is extended about 3 km into the sea to provide 3 m draft at low tide. Note that tidal range in Chabahar Bay area is about 2 m. The northern shoreline of the bay is directly exposed to incoming south waves. A water desalination plant with an intake structure has been constructed in this part.

2. Monitoring Program

As the first phase of a series of monitoring and modeling studies of Iranian coastal areas, the entire Chabahar Bay was under a comprehensive monitoring and modeling study in 2006-2007. The study included site visits, overflight, analysis of historic airphotos and charts in GIS, hydrographic and topographic surveys, a 22-year wave hindcast, sediment sampling, multi point measurements of waves and hydrodynamics for a full year and various 2DH and 3D numerical modelling of hydrodynamics and sediment transport. The extensive one-year field measurements program was designed to provide the inputs or boundary conditions and the validation data for numerical models. The one-year monitoring program included wave and current measurements at seven stations, tide measurements at three stations, offshore wave measurements using a PMO (Port and Maritime Organization) buoy and wind measurements. An analysis of the collected hydrodynamic data and the results of 3D numerical modeling are described in this paper.

2.1. Deployed Instruments

Three Nortek AWAC Acoustic Doppler Profilers (ADP), namely AW1, AW2 and AW3, were deployed at the entrance of the bay and vicinity. AW1 was located near Shaheed Beheshti Port breakwater, AW2 at 28 m water depth east side of the entrance to the bay and AW3 at the west end of the bay entrance. A directional wave buoy was deployed at 30 m depth outside of the bay near AW2. The buoy and AW2 both measured deepwater wave parameters. Locations of the three AWACs were fixed during the one-year campaign.

Additionally, Nortek Aquadopp and Vector current meter units were used for current and wave measurements in the nearshore. Two tide gages TG2 and TG3 were deployed in Ramin and Iranbandar ports, located outside on both east and west sides of the bay, to provide water level boundary conditions for the hydrodynamic model.Although two permanent

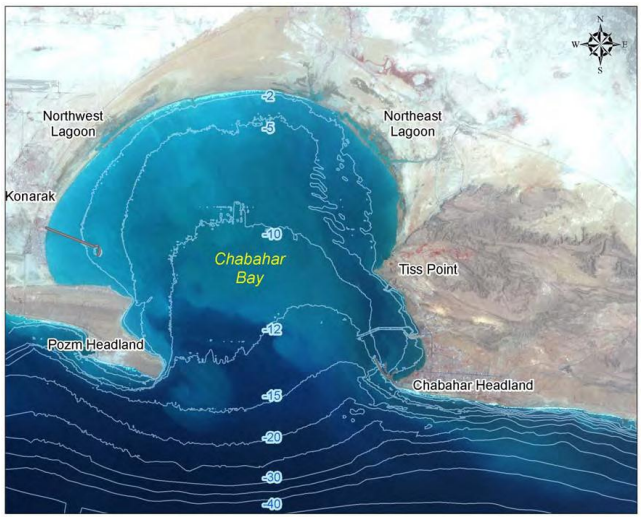

Figure 2. Bathymetry of Chabahar Bay

synoptic wind stations were operating in the area, a new wind station was set up at the southeast corner of the bay on the land because of the complex pattern of the local topography. Locations of the Vector and Aquadopp instruments were changed a few times during the measurement period to cover as much of the study area as possible and to provide required data for model calibration/verification purposes. Figure 3 shows the arrangement of instruments in February 2007 as an example.

It is noteworthy to add that tropical cyclone Gonu attacked the study area in early June 2007. The cyclone damaged the anchorage system of the offshore wave buoy and some of the instruments, located in shallow waters, could not resist the large storm waves. However, several other instruments deployed in relatively deeper water successfully captured the waves and currents induced by cyclone Gonu from June 1 to 7, 2007 (Dibajnia et al., 2010).

2.2. Hydrodynamic Measurement Results

Figure 4 shows a summary of measured winds at two synoptic permanent wind stations and the established station around the bay. The differences of wind roses reveal the local effects of the high elevation lands that result to a complex local wind pattern in the area. Figure 5 shows an example of the one-month current roses measured during March, 2007. It is observed that the tidal currents entering the bay mostly follow the shoreline direction. Figure 6 is a snapshot of the velocity vectors measured by ADPs at 5 horizontal layers. A remarkable difference is observed between the magnitude and the direction of current vectors at each location. This reveals the complex 3D pattern of currents indicating the necessity of employing 3D numerical models to simulate the phenomena. The direction of the near surface current was highly affected by the wind direction at the time of measurement. A one-year summary of current roses measured at the middle layer is shown in Figure 7. It

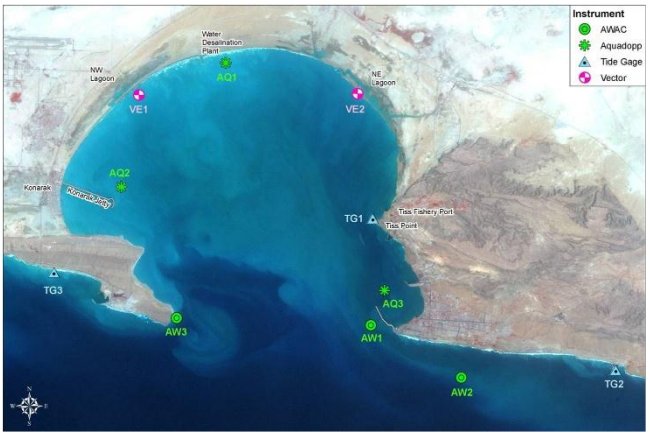

Figure 3. Locations of deployed instruments in February 2007 (AW refers to an AWAC, AQ refers to an Aquadopp and TG refers to a Tide Gauge)

Figure 4. Measured wind roses around Chabahar Bay

should be noted that the duration of the measurements at some locations was less than one year.

3. Hydrodynamic Modelling of Chabahar Bay

3D modeling of coastal hydrodynamics generally becomes important when dealing with stratified flows or when wind blows over shallow water basins. Wind driven currents are created by the wind exerting stress on the sea surface. This stress causes the surface water to move, and this movement is transmitted through vertical mixing to the underlying water to a depth that is dependent mainly on the strength and persistence of the wind. In some coastal areas of the ocean (and large lakes), the combination of persistent winds, Earth's rotation (the Coriolis effect), and restrictions on lateral movements of water caused by shorelines and shallow bottoms induces upward and downward water movements.

The current profiling considered in the present field measurement program revealed part of the bay-wide circulation mechanism. However, numerical modeling is required to determine the full spatial picture of such a circulation and its sensitivity to environmental factors such as tides and winds.

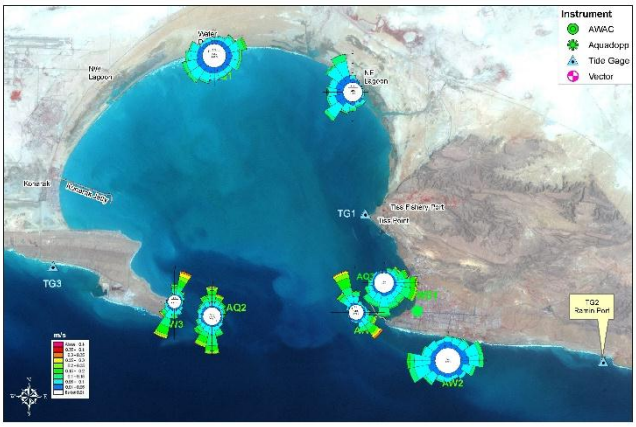

Figure 5. Current roses of the upper Cell, March 2007

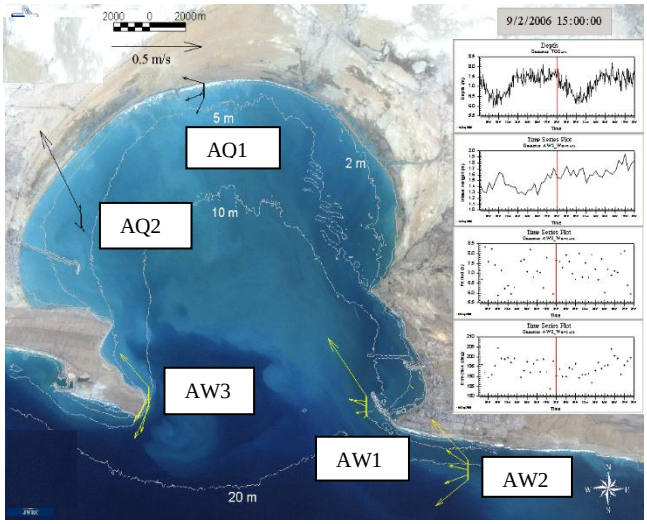

Figure 6. A snap shot of velocity vectors measured by ADPs at different layers

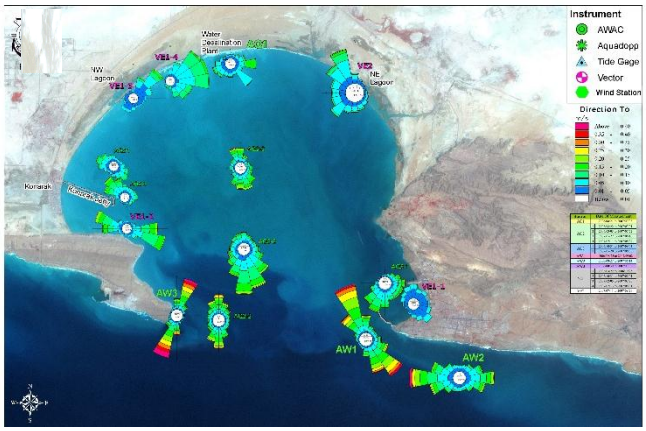

Figure 7. Summary of current roses of the middle cell (August 2006 to August 2007)

3.1. MISED 3D Model

MISED is a 3D numerical hydrodynamics and sediment transport model for simulation of hydrodynamics, temperature, salinity, sediment transport, and morphology in rivers, estuaries, and coastal areas (Lu and Wai, 1998). In this model, the Navier-Stokes equations for shallow water with the hydrostatic pressure assumption are transformed from the Cartesian coordinates to Sigma coordinates. The momentum equations for 3D shallow water currents consist of advection, horizontal and vertical diffusion, Coriolis force, and pressure gradient terms. A Hybrid Operator Splitting (HOS) method is used to provide efficient and stable 3D computations in shallow water. The method divides the momentum equation into three parts, which are then solved in three time sub steps. The Eulerian-Lagrangian approach is used to solve for advection and Coriolis force in the first time sub step, while the standard implicit Galerkin FEM (Finite Element Method) is used to discretize the horizontal diffusion in the second time sub step. In the third (last) time sub step, the vertical diffusion and pressure gradient are discretized using implicit FDM (Finite Difference Method) for each nodal column. The continuity equation is also solved in this time sub step by implicit FEM for the free surface elevation. The highlighted numerical features of MISED are:

• Unconditional stability - the method was theoretically proved to be unconditionally stable. That is, the model allows using much larger time steps than other 3D models such as ADCIRC3D, CH3D, and DHI MIKE3. In fact, typical time steps used in the model are more than ten times larger than other models for the same grid size;

• High computational performance – computation time has been minimized through the use of optimized numerical schemes, solution of linear system of equations and program coding. Therefore, the model can be applied to the long-term simulation of physical processes;

• Second order accuracy – the model uses second order interpolation function for nine node quadrilateral finite elements in horizontal plane;

• Drying and wetting process: The model can be used to estimate the flooding situation in rivers, lakes and coastal areas. The model adopts the natural flooding paths, that is, flood from the lower land to high land with limited hydraulic speed, to process the states of drying and wetting elements. The drying and wetting process is embedded into the system for solving the continuity equation so that mass conservation is satisfied in each element without requiring extra computational time.

3.2. Model Setup

An initial hydrographic survey of Chabahar Bay was conducted by Iranian National Cartographic Center (NCC) in 2006. Depth contours were digitized from the 1992 1:100,000 scale National Geographic Organization Chart to add the areas not covered in the 2006 hydrographic survey and also to extend the model bathymetry to offshore boundary at 50 m water depth. High water line was determined from the 2005 QuickBird satellite imagery. Specific control point nodes were defined at various points around the shoreline, particularly at changes in shoreline orientation and where a change in the grid density was

desired. Once the control nodes were defined, the grids were generated in horizontal plane using nine-nodal finite quadrilateral (grid cell). The MISED model calculates the hydrodynamics at each node. After the cells were established the bathymetry was interpolated to the model grid nodes directly from the raw survey points. The entire model domain is shown in Figure 8. It is worth noting that locations with steep slopes required adjusting the position of control nodes to force generation of more grids and inclusion of the bathymetry.

Each cell was brought into three dimensions by breaking it into eleven evenly distributed layers through the water column. This results in greater resolution in shallower areas, where wind-driven surface currents result in more variation in the vertical structure of hydrodynamics. Calibration runs were undertaken with 21 layers, however there was little improvement made for the significant increase in model run-time and as a result it was decided to stay with eleven layers. Initial runs were completed in MISED using simplified conditions to determine the stability of the grid model, and minor adjustments made. A finer grid size had to be used near the shoreline for simulation of wetting and drying to avoid model instability. Using finer grids resulted in significant increase in calculation time. As wetting and drying was not a key factor in the present simulations, it was decided to discard this process in the present modeling work. This was achieved by lowering the elevation of the shore boundary of the model (i.e. the high water line) such that it is always submerged.

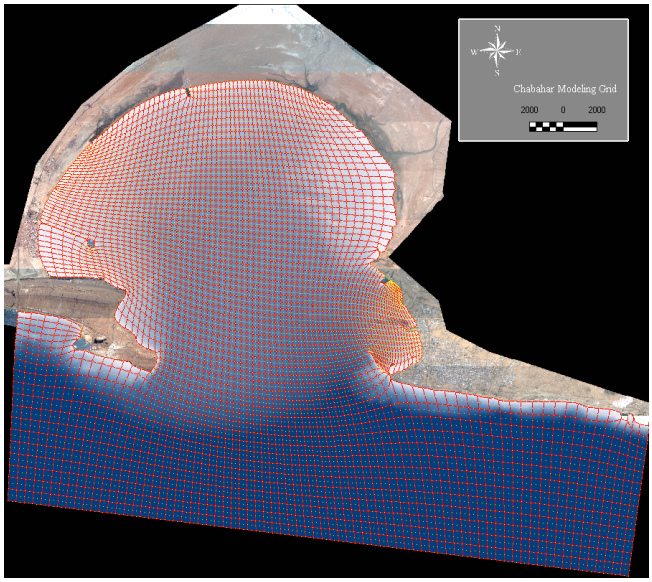

Figure 8. Entire model domain grid cells overlaid on bathymetry

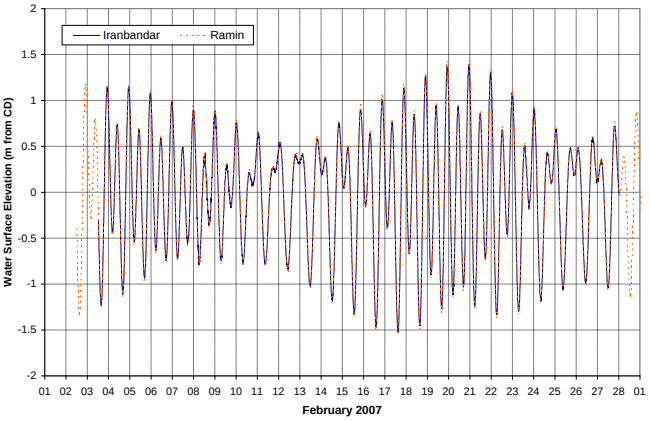

Figure 9. Water surface elevations at the model lateral boundaries

3.2. Boundary Conditions

Through the understanding of the tides in the vicinity of Chabahar Bay, a number of different configurations were tried with regards to the offshore boundaries in this study. The first approach was to keep the east and west lateral boundaries open, while closing the southern offshore boundary (i.e. a wall boundary). It was believed that tides cycle through this area from the east to the west, and this configuration would force the model to interpret surface elevation changes along the south boundary in this way. Surface elevations recorded at Ramin (TG2) were used for the eastern lateral boundary condition, and surface elevations recorded west of Iranbandar (TG3) were used for the western lateral boundary condition. Figure 9 shows the input water surface elevations at Ramin and Iranbandar lateral boundaries during the month of February. Tides are semi-diurnal at Chabahar with 12.4-hour periods. There are two high tides (i.e. high high tide and low high tide) and two low tides (i.e. low low tide and high low tide) in each day. Spring tides and neap tides happen alternatively every 2 weeks. Spring tide is the tide with higher highs and lower lows at full moon and new moon. Neap tide is the tide with less amplitude at the end of the first and last quarters. Neap tides are observed as nearly diurnal tides for a few days around February 13 and February 26.

After initial model testing, it was decided that wind-driven surface currents might not be properly simulated with a closed offshore boundary. Surface currents are generated immediately in response to the applied wind field. When the wind was towards the offshore boundary (south), the corresponding surface current was blocked by the wall, resulting in unrealistic undulations in the velocity field along the boundary. Thus the southern offshore boundary was changed to a Zero-Net-Flux (ZNF) boundary in an attempt to better model wind-driven currents. The ZNF boundary allowed surface currents to flow out of the calculation domain while introducing a return flow in the bottom layers to keep the net flux zero. In this way, there was still no tidal flow through the southern offshore boundary which was handled as a linearly varying surface elevation gradient between the eastern and the western boundaries. The eastern and western boundaries remained as the recorded surface elevations from Ramin and Iranbandar, respectively.

The results showed that the flow was converging from lateral boundaries into the bay during the rising tide while it flowed out of the bay diverging towards the lateral boundaries during the falling tide. There was not a predominant east to west or west to east flow pattern as initially speculated. Under these conditions, therefore, the flow pattern obtained under the ZNF boundary conditions is somewhat unrealistic and one would as well expect tidal flow to happen through the offshore boundary. It was thus decided to use open boundary conditions for the southern offshore boundary to allow tidal flow through this side of the model domain.

3.3. Model Calibration

3.3.1 Bottom Roughness

Bottom roughness is influenced by nearshore bathymetry, sediment grain size, geology, vegetation, and bed forms. The bottom in the study area, however, does not represent many features and it is not necessary to vary the roughness spatially throughout the entire model domain. A constant bed roughness (n_{min}) of 0.017 was used in the initial runs resulting to a general underestimation of the modeled velocities near the bed. Increasing the base roughness (n_{min}) to 0.05, and allowing for a further increase with decreasing water depth resulted in an improved agreement between near-bottom measured and calculated velocity. While this seems counter-intuitive, increasing the roughness results in an increase in the amount of turbulence near the bottom. Thus the boundary layer becomes thinner (the viscous sub-layer disappears), resulting in an increase in near-bottom velocity. This is in contrast to conventional 2D modeling, where decreasing the bed roughness results in increased depth-averaged velocity.

3.3.2 Wind Stress Conversion

The moving air (wind) applies a stress to the water surface, pushing the water in the direction of the wind. This energy is transmitted down into the water column through vertical mixing. The wind shear stress is simply assumed to be proportional to square of wind velocity through using the wind drag coefficient. The drag coefficient depends on the wind speed and increases with increasing wind speed. It is necessary to calibrate the wind shear stress or drag coefficient to match measurements. Typical values for the drag coefficient range between 0.0015 and 0.0065. The measured wind by the deployed wind station was uniformly applied over the entire domain. Calibration results were compared using several specific wind events. Some difficulty was observed with respect to the directionality of the wind events, particularly in matching the surface velocities at all of the stations. It is believed that this difficulty stems from the land effect. For example, at AW3 it is not possible to simulate surface velocities for wind events coming from the West; the relatively high Pozm Headland blocks the west wind resulting in a non-uniform wind field not simulated in MISED. Therefore, during review of wind results, the directionality of the wind event was taken into account relative to the station being considered. A final challenge with wind calibrations is that the velocities are also constantly influenced by the tides: a wind event that occurs during a falling tide will produce a different surface velocity than if the same wind event occurs during a rising tide. Comparison of several model runs with different drag coefficient resulted in selection of 0.002 for the wind shear stress coefficient as it produced the most realistic results.

3.3.2 Turbulence Parameters

Horizontal and vertical eddy viscosity coefficients are important parameters for turbulence mixing. Turbulence mixing is generally larger in places where the velocity gradient is large. MISED is capable of using several different turbulence models. There are 3 options for horizontal eddy viscosity: 1) a constant eddy viscosity, 2) Smagorinsky (1993) eddy viscosity which is a function of velocity gradients, and 3) solving the two closure k-ε equations. Similarly, there are 4 options for vertical eddy viscosity: 1) constant, 2) parabolic, 3) parabolic-constant and 4) solving the two closure k-ε equations.

Considering the large extent of calculation domain, solving k-ε equations results in extremely long calculation times that were considered impractical. Therefore, the Smagorinsky eddy viscosity was used for horizontal turbulence. For the vertical eddy viscosity, both parabolic and parabolic-constant types were examined. The parabolic type resulted in a better match in velocity magnitudes at both the surface and the bed.

3.3.3 Calculation Time Step

MISED uses an unconditionally stable algorithm, which allows using large calculation time steps (up to 3600 s) for tidal current calculations with minimal loss of accuracy. For simulation of wind-driven currents, however, the accuracy depends on the applied time step. Previous modeling experiences and comparison with analytic solutions indicate that a time step of 60 s is most appropriate for simulation of wind-driven currents. Further reduction of the time step did not result in noticeable improvements. A time step of 60 s was therefore used for the present calculations.

3.4. Model Results and Comparisons

Simulations were completed for the months of February and March 2007 and the results were compared with the AWAC measurements. The deployment locations for the AWACs are shown in Figure 3. Input to the model consisted of water levels along the east and west lateral boundaries and the

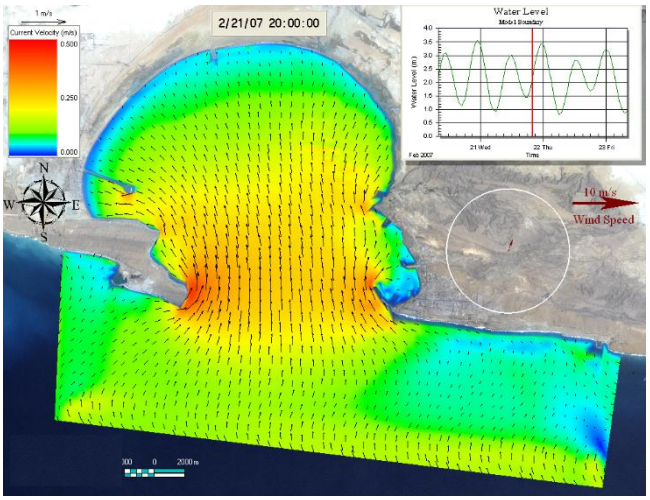

Figure 10. An example of calculated surface velocity vectors at flood tide with offshore open boundary condition

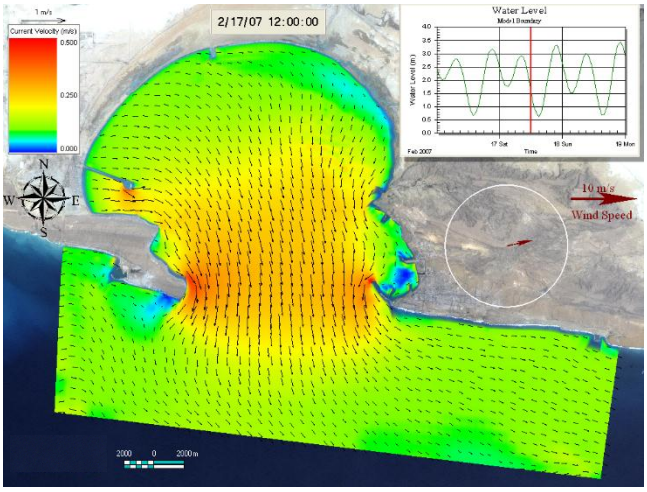

Figure 11. An example of calculated surface velocity vectors at ebb tide with offshore open boundary condition

wind uniformly over the entire domain. Figure 10 is an example snapshot of surface velocity vectors during rising (flood) tide on February 21. Figure 11 shows snapshot of surface velocity vectors during lowering (ebb) tide on February 17. Winds were insignificant in both cases and tidal currents were predominant. Tidal currents outside Chabahar Bay during the ebb event were from west to east. There was no clear corresponding tidal current direction during the flood tide event. Figures 10 and 11 indicate that in the absence of strong winds, sea water flows in and out of Chabahar Bay all across the bay entrance during flood and ebb tides, respectively. The impact of wind-driven currents is discussed in the next section.

Figure 12 shows an example of comparisons between calculated water surface elevations and tide gauge measurements at TG1 near Tiss Fishery Port inside Chabahar Bay between February 17 and 22. It is observed that both tidal amplitude and phase are properly simulated. The model underestimates the tidal amplitude by a few centimeters, but this is within the accepted error range for this type of modeling (less than 10 cm). The underestimation is mainly

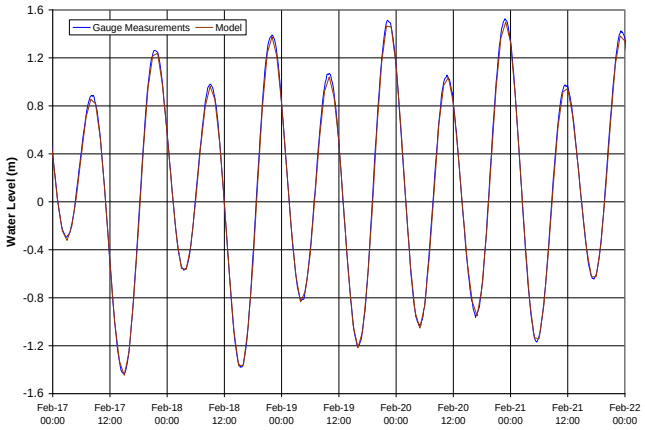

Figure 12. Comparison of measured and calculated water surface elevation at TG1

contributed to application of the large bottom friction factor. Similar agreements between predicted and measured water surface elevations were observed at other locations.

Figure 13 shows comparison of predicted and measured velocity vectors (quiver plots) during the neap tide from February 15 and 20, 2007 at AW1. The top graph shows variation of water level as measured by the pressure sensor of AW1. The second graph shows the measured wind velocity vectors. The remaining three graphs show comparison of measured (red) and calculated (black) velocity vectors near the surface, at the mid depth and near the bottom, respectively. The agreement between model and measured results is good, although the calculated direction of outgoing ebb tide velocity is somewhat different from the ADP measurements, which are more towards the breakwater or eastward. This is attributed to possible generation of an eddy on the west side of the breakwater during the ebb tide. The ebb velocity of a spring tide is large resulting in generation of an eddy behind the Shahid Beheshti breakwater. This eddy was not simulated in the model because of the relatively coarse grid size around the breakwater. Figure 14 shows similar results at AW1 between March 12 and 17, 2007 when the tide was completely semi-diurnal. A very good agreement in both magnitude and direction of velocities is observed. Winds from the SE were predominant in this period and resulted in increased ingoing flood velocity and reduced outgoing ebb velocity. Similar comparison quiver plots were done for other instruments during February and March, 2007.

Figure 15 shows comparison of measured and calculated velocity magnitudes (speed) at AW1, AW2 and AW3 for the February 15 to 20 period. The top graph in this figure shows variation of water level as measured by AW1. The next graph shows wind speed and direction. The third graph presents comparison of measured and calculated velocity magnitude at 3 different levels at AW1. This graph corresponds to figure 13 and presents a reasonable agreement

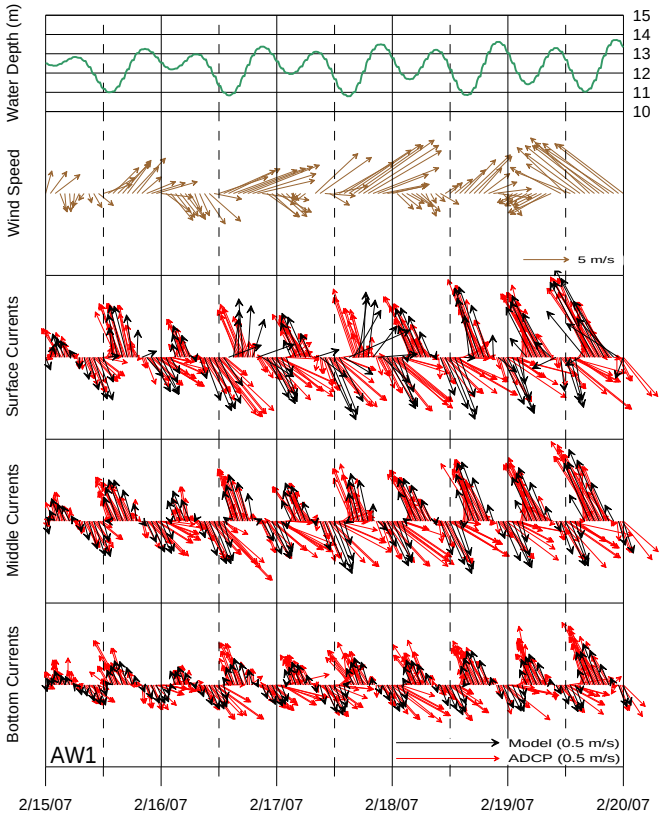

Figure 13. Velocity comparison quiver plots at AW1 for February 15 to 20, 2007

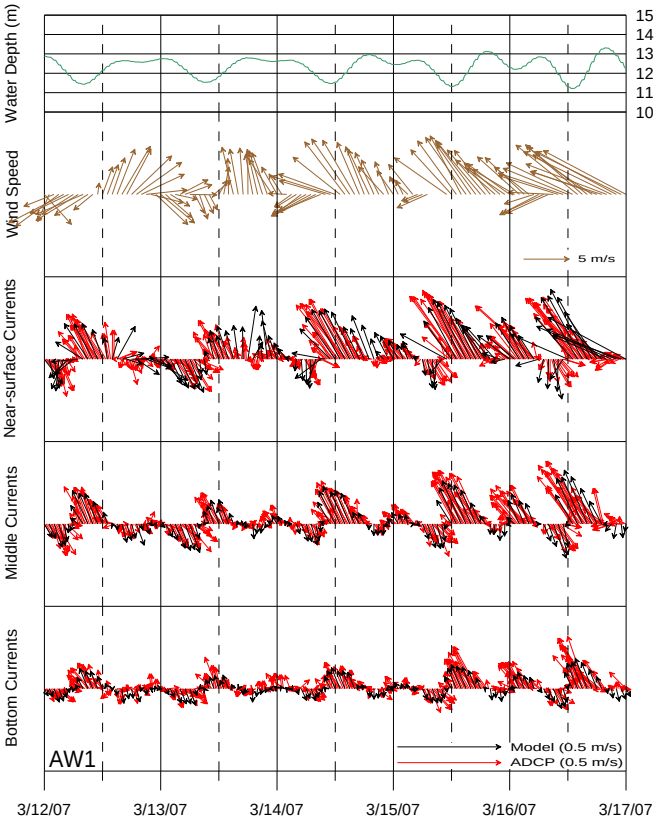

Figure 14. Velocity comparison quiver plots at AW1 for March 12 to 17, 2007

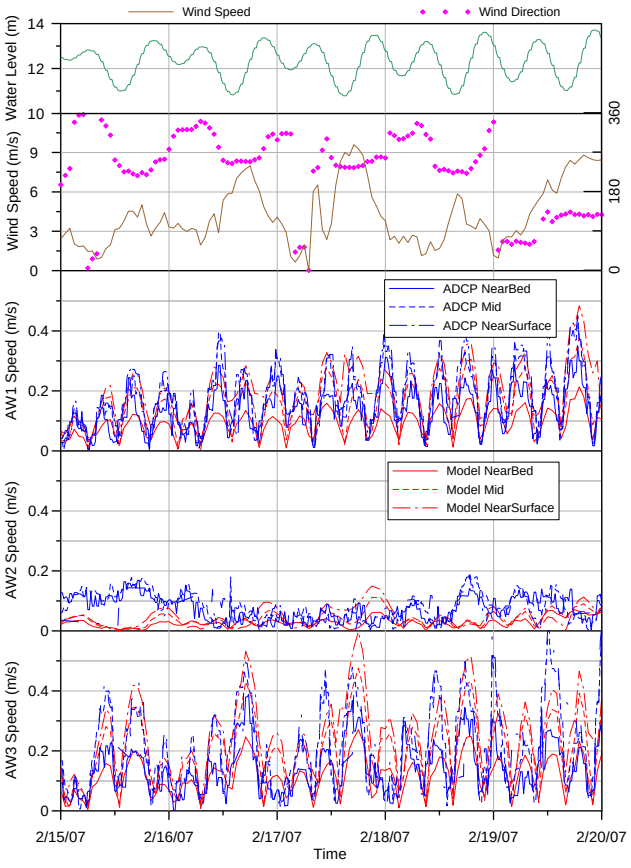

Figure 15. Comparisons of measured and calculated velocity magnitude at AW1, AW2 and AW3 during February 15 to 20, 2007

between measured and calculated results. The next graph presents a similar comparison at AW2. AW2 was deployed in 28 m water depth outside of Chabahar Bay (Figure 3). The water at this site was very clean and AW2 could hardly measure currents beyond a distance of 20 m from the bottom. Therefore, the near-surface velocity is about 8 to 10 m below the surface for both model and measurements. Generally, velocity magnitudes are small at AW2 and the model is doing a reasonably good job, although seems to be missing some events on February 15. These events, however, are believed not to be tidal related. It should be noted that the velocity predicted by the model for near the actual surface directly responds to wind events. The bottom graph in Figure 15 shows the comparison at AW3, which was deployed in the west end of the bay entrance (Figure 3). Generally the velocity at all levels is very well simulated. Winds in this period blew mostly from west. They did not have significant effect on surface velocity at AW3 as the sensor was in the area sheltered by Pozm Headland. Similar comparisons were conducted between the measured and calculated velocity magnitudes (speed) at AQ1, AQ2 and AQ3 for the periods in the months of February and March with satisfactory results.

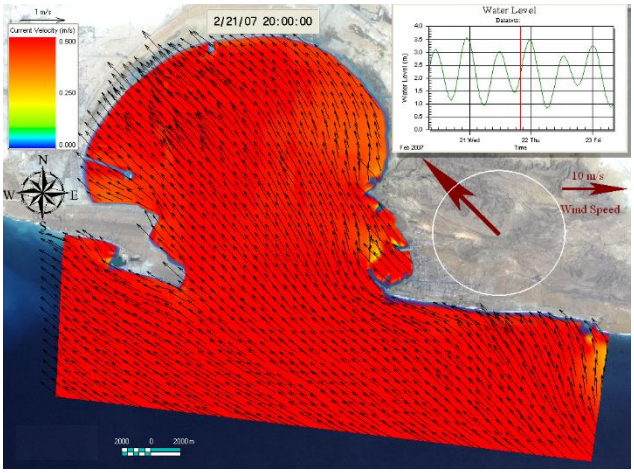

Figure 16. Example of calculated surface velocity vectors at flood tide with an imaginary 15 m/s wind from southeast

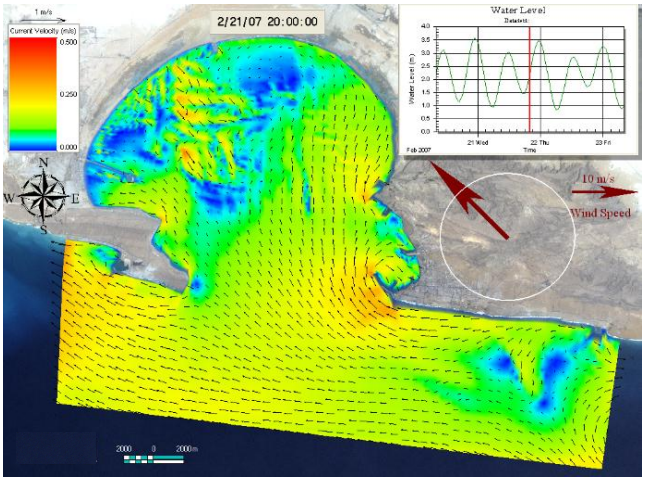

Figure 17. Example of calculated near-bottom velocity vectors at flood tide with an imaginary 15 m/s wind from southeast

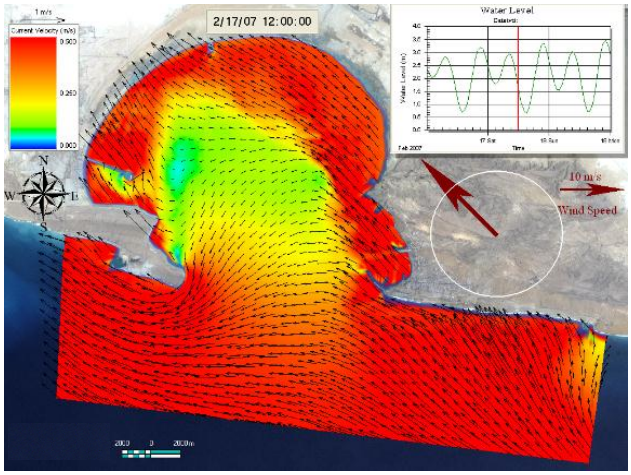

Figure 18. Example of calculated surface velocity vectors at ebb tide with an imaginary 15 m/s wind from southeast

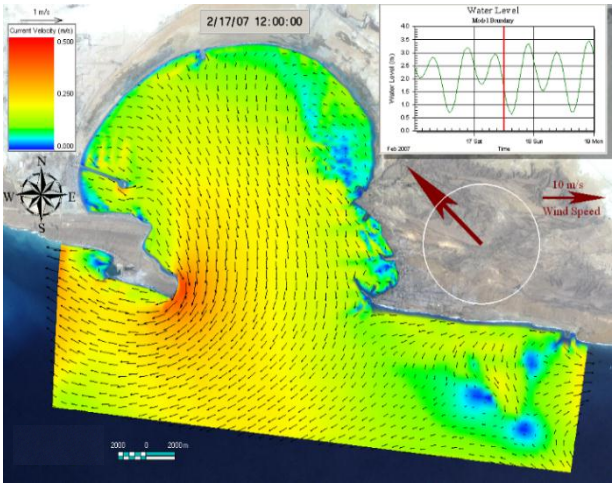

Figure 19. Example of calculated near-bottom velocity vectors at ebb tide with an imaginary 15 m/s wind from southeast

3.5 Wind effect

Winds can significantly modify surface currents and result in dramatic changes in vertical flow structure. In order to illustrate the effect of winds on current velocities in Chabahar Bay, two hypothetical MISED runs were completed. In these runs, the measured water surface elevations at Ramin and Iranbandar in February were used as boundary conditions. For the winds, however, a constant wind speed of 15 m/s from SE direction was applied. These are the most predominant wind directions according to Chabahar synoptic station long-term wind data. It was found that surface currents may be considerably modified by the wind and generally follow the wind direction. Near-bottom tidal currents, on the other hand, are considerably modified to compensate for the extra water mass brought into the shore by the wind-driven surface currents.

Figure 16 shows calculated surface velocity vectors with the constant SE wind for the rising tide event on February 21, 2007. This figure should be compared to Figure 10, which shows simulation results with the actual but negligible winds. Surface currents are considerably modified by the wind and follow the wind direction. Figure 17 shows the calculated velocity vectors near the bottom. Near-bottom flood tidal currents are considerably modified across the bay and particularly on the northwest corner where the currents are towards the central bay to compensate for the extra water mass brought into the shore by the wind-driven surface currents.

Figure 18 shows calculated surface velocity vectors with the constant SE wind for the falling tide event on February 1, 2007. This figure should be compared to Figure 11, which shows simulation results with the actual but negligible winds. In Figure 18, surface currents enter the bay near the Shahid Beheshti breakwater and flow out of the bay at the other end of entrance by the Pozm Headland. Figure 19 shows the calculated velocity vectors near the bottom for the same event. Near the bottom, everywhere across the entrance, the bay is discharged into the Gulf of Oman. At the west end of the entrance by the Pozm Headland (location of AW3), therefore, there would be outward flow throughout the water column under persistent SE winds at the time of falling tide.

The simplified situation described in Figures 16 to 19 is similar to June 2007 when cyclone Gonu attacked the area. Cyclone Gonu lasted from June 1 to 7, 2007,

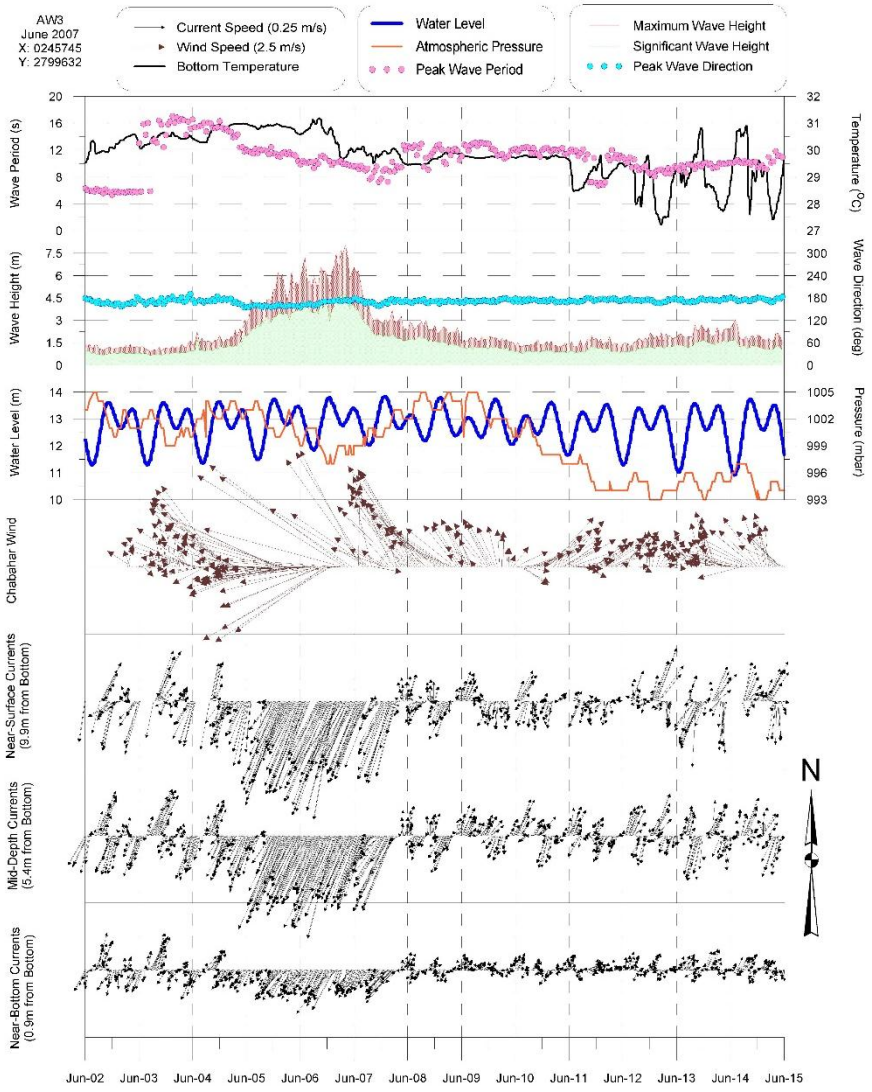

Figure 20. Waves and currents measured by AW3 in June 2007

and was the most intense tropical cyclone on record in the Arabian Sea. During cyclone Gonu event, AW3 recorded persistent SSW currents for more than 2 days. A maximum wind speed of 16 m/s from SE direction was measured in the evening on June 6. Measured data are summarized in Figure 20 which in order from top to the bottom presents water temperature and wave period, wave height and wave direction, water levels and air pressure, wind speed vectors, and measured current velocity vectors by the instrument at three levels (near the surface, mid-depth and near the bottom). The outgoing SSW current occurred from mid-day June 5, to around mid-day June 7. During the same period, very strong westward currents were recorded at AW2 outside of the bay. Strong winds were persistently blowing initially from east and then from southeast in the above period. It is likely that the strong wind-driven westward current outside of the bay entered the bay near Chabahar headland and flowed out by the Pozm headland, similar to what is shown in Figure 18. The current was very strong and overshadowed local tidal currents at AW3.

3.6 Particle Tracking

Simulations of particle movements were completed by a Lagrangian Particle Tracking Model (LPTM), which operates upon objects having UV or UVW vector components that are fully specified both temporally and spatially. The model employs a Gaussian random-walk dispersion using velocities that are interpolated both spatially and temporally. The overall transport of the particles during a time interval results from an advective component and a dispersive component, which represents sub-grid flow processes and turbulence. The vertical variation of the currents advecting the particles in the horizontal plane at a given height above the bed is defined on the basis of the typical logarithmic profile. The downward movement of the particle (if included) is a randomized function of the input settling velocity. The settling option permits the vertical movement of particles due to gravity when transported by a vertically-averaged current field.

Particles were released at the water surface at all grid points over the entire calculation domain (Figure 21).

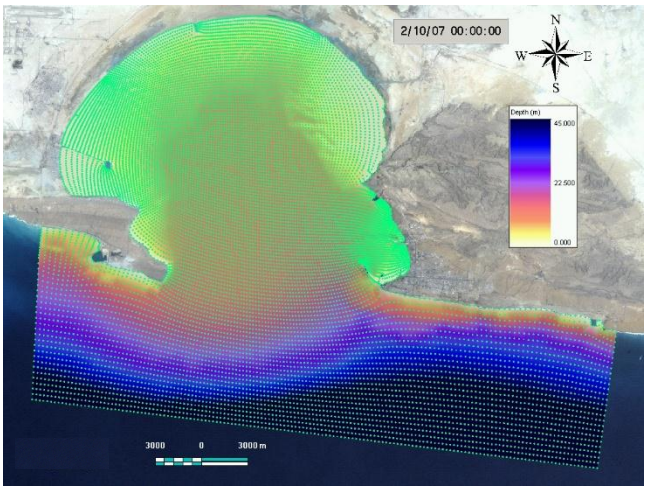

Figure 21. Particle injection points for particle tracking

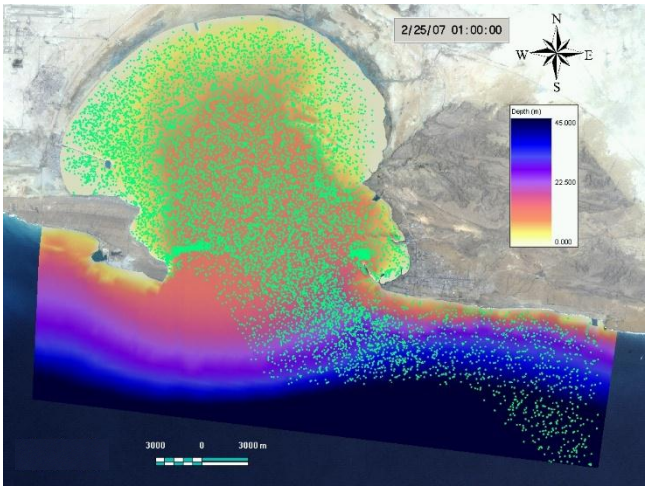

Figure 22. Final distribution of particles under tides (February 2007)

Settling velocity and decay rate were set to zero. A particle was therefore assumed to be buoyant and would leave the calculation domain only when it hits any of the model boundaries. Particle tracking was completed with MISED results for the month of February with and without winds (tides only) as input driving force. Figure 22 shows the final distribution of the released particles under the action of tides, while Figure 23 presents the corresponding results when both winds and tides are considered. From Figure 22 there seems to be a net flux of particles under the tides outside of the bay over the simulation period. The direction of the net movement is from west to east. Inside of the bay, however, the particles do not show any considerable redistribution compared to their original positions. Figure 23, on the other hand, shows the final distribution of particles when winds (and wind-driven currents) are also taken into account. Winds in general have worked to push the particles out of the bay over the simulation period. Figure 24 shows the July 17, 2000 Landsat image of Chabahar and Pozm bays with emphasis on band 2 color over the water. The yellow color in this figure is likely an indication of suspended matter near the

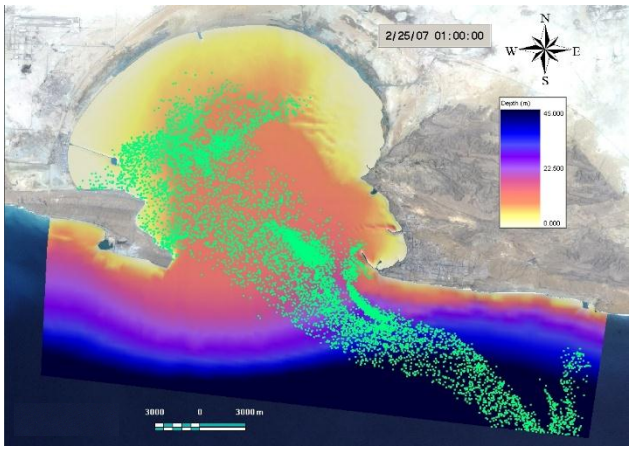

Figure 23. Final distribution of particles under tides and wind-driven currents (February 2007)

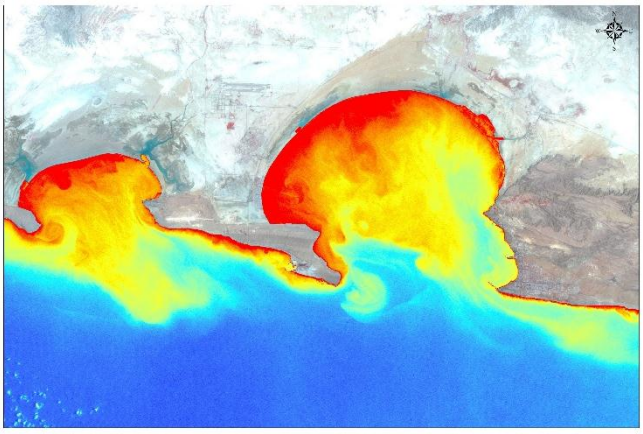

Figure 24. Landsat image of Chabahar area with emphasis on color band 2

water surface and represents a snap shot of a bay-wide circulation created by winds and tides. Winds in July are typical of the winds in monsoon season and blew mostly from SSE to SE directions. The particle distribution pattern in Figure 23 is very similar to the pattern observed in the satellite image of Figure 24, in which there seems to be an outgoing flow towards SE direction. Outside of the bay, the suspended plume was being transported to the east.

5. Conclusions

A comprehensive one year dataset of waves and currents of Chabahar Bay was collected. The data indicates that the tidal currents mostly enter the bay at the eastern headland and exit at the western part. Tidal circulations inside the bay during each tidal cycle had a complex pattern different from the previous tidal cycle.

MISED 3D hydrodynamic numerical modeling was completed for Chabahar Bay for February and March 2007 and the results were compared with the measurements at several locations with satisfactory agreement. Particle tracking simulations showed that wind-driven currents are responsible for carrying suspended material out of the bay. Winds at Chabahar are mostly from SW to SE directions. Strong winds

from these directions create near-bottom currents inside the bay that tend to carry suspended particles from NW and NE sides of the bay towards central bay area and from there gradually to outside of the bay. The combination of winds and tides, therefore, has a very important flushing function for water quality of Chabahar Bay. In other words, the assimilative capacity of the bay is enhanced by the flushing associated with the effect of winds and tides in driving offshore flows.

It should be added that the present hydrodynamic model did not include the forces due to wave-induced radiation stresses. Therefore, wave-driven nearshore currents that generally occur along the shoreline inside the surf zone were not calculated. Discarding nearshore currents had potential impacts on comparisons with data from the shallow water nearshore sensors (i.e. Vectors). However, comparisons between the model results and measured currents at the three AWACs and other instruments deployed outside of the surf zone measuring the bay-wide circulations are not influenced.

In summary, the Hydrodynamics of Chabahar Bay was found to be generally complicated and dominated by tidal and wind-driven currents. Winds can significantly modify surface currents and result in dramatic changes in vertical flow structure. Surface currents are considerably modified by the wind and follow the wind direction. Near-bottom flood tidal currents across the bay are also highly influenced by the winds and particularly on the northwest corner where the currents are towards the central bay to compensate for the extra water mass brought into the shore by the wind-driven surface currents. More accurate simulation of wind-driven currents requires application of a spatially variable wind field over the bay.

Acknowledgment

The authors are grateful to the colleagues at Jahad Water and Energy Research Company (JWERC), Darya Negar Pars (DNP) and Baird companies for their contributions in field measurements and modeling. Thanks are extended to the Ports and Maritime Organization for the support of the conducted research through the 1st phase of monitoring and modeling studies of Iranian coastlines.

8. References

1- Dibajnia M., Soltanpour M. and Scott D. (2010), An assessment of climate change impact on cyclone frequency and design wave height in the Oman Sea, *1st WMO International Conference on Tropical Cyclones and Climate Change*, World Meteorological Organization Technical Notes, WWRP 2010-2, pp. 19-28

2- Duing, W. (1970), The monsoon regime of the currents in the Indian Ocean. *East west Centre Press*, University of Hawai, Honolulu, 68 p.

3- Falcon, N.L. (1947), Raised Beaches and Terraces of the Iranian Makran Coast. *Geographical Journal*, 109, pp. 149-151.

4- Flagg, C. A. and Kim, H.-S. (1998), Upper ocean currents in the northern Arabian Sea from shipboard ADCP measurements collected during the 1994–1996 U.S. JGOFS and ONR Programs. *Deep-Sea Res. II*, 45, pp. 1917–1959.

Le Blond, P. H. (1979). An explanation of the logarithmic spiral plan shape of headland-bay beaches, *J. sedimentary petrology*, 49(9), pp. 1093-1100.

5- Lu, Q. and Wai, O.W.H. (1998), An Efficient Operator Splitting Scheme for Three-Dimensional Hydrodynamic Computations, *Int. J. Numer. Meth. Fluids*, Volume 26, pp. 771-789.

6- Rea, C. C. and Komar, P. D. (1975), Computer simulation models of hooked beaches shoreline configuration, *Journal of Sedimentary Research*, 45(4), pp. 866-872.

7- Reyess, J. L., Pirazolly and P. A., Haghipour, A. (1998), Quaternary Marine Terraces and Tectonic Uplift Rates on the South Coast of Iran. *Centre des Faibles Radioactivites* (*CNRS-CEA*), pp. 225-237.

8- Shankar, D., Vinayachandran, P. N. and Unnikrishnan, A. S. (2002), The monsoon currents in the north Indian Ocean, *Progress in oceanography*, Volume 52, No. 1, pp. 63-120.